Journal of Molecular Catalysis A: Chemical 425 (2016) 190–198

Contents lists available at ScienceDirect

Journal of Molecular Catalysis A: Chemical

journal homepage: www.elsevier.com/locate/molcata

Research Paper

Production of high-calorie synthetic natural gas using copper-impregnated iron catalysts

Yong Hee Lee [a], Dae-Won Lee [b,**], Kwan-Young Lee [a,c,*]

[a] Department of Chemical and Biological Engineering, Korea University, Anam-dong, Seongbuk-gu, Seoul 02841, Republic of Korea
[b] Department of Chemical Engineering, Kangwon National University, 1 Kangwondaehak-gil, Chuncheon-si, Gangwon-do 24341, Republic of Korea
[c] KU-KIST School of Converging Science and Technology, Korea University, Anam-dong, Seongbuk-gu, Seoul 02841, Republic of Korea

ARTICLE INFO

Article history:
Received 26 July 2016
Received in revised form 6 October 2016
Accepted 9 October 2016
Available online 12 October 2016

Keywords:
High-calorie synthetic natural gas
Fe-Cu catalyst
Heating value

ABSTRACT

Fe-Cu catalysts were applied in the production of high-calorie synthetic natural gas (HC-SNG), wherein a proper level of C_2–C_4 hydrocarbon selectivity must be secured. The Fe-Cu catalysts were activated by reduction under diluted CO gas before the reaction, and their catalytically active Fe phases changed according to the reduction temperature: Fe_3O_4 formed when reduced at 300 °C, carbon-deficient FeC_x at 400 °C and Fe_3C at 500 °C. Iron carbide catalysts achieved stronger CO adsorption and higher BET surface area than Fe_3O_4 catalysts, which resulted in higher CO conversion. The carbon-deficient FeC_x was metal-like in its electron structure due to the low number of bonded carbons, and it was attributed to the highest CO and H_2 conversion of FC15-400R by providing H_2 activation ability. The C_n ($n \geq 2$) selectivity or carbon chain growth of the hydrocarbons increased as the carburization degree of the active Fe phase increased, which was associated with an increase in the CO chemisorption strength. The impregnated Cu exerted little influence on the product selectivity, but it promoted hydrogen adsorption, thereby improving the paraffin-to-olefin ratio of the produced hydrocarbons.

1. Introduction

Natural gas is still regarded as the most promising alternative fossil fuel resource for petroleum. It is estimated that the global production of natural gas will increase from 632 billion m^3 in 2013 to 1667 billion m^3 in 2040 [1]. The reserves-to-production ratio (R/P), which indicates the remaining time (or amount) to depletion for a fossil fuel resource, is estimated to be 54.1 years for conventional natural gas [2]. However, as unconventional resources such as shale gas, tight gas, coalbed methane, and methane hydrate are discovered, the R/P value of natural gas is extended, making it one of the most important issues in energy industry. In addition, the use of natural gas is recommended because it has environmental advantages over the use of other fossil fuel resources. Because methane has the highest H/C atomic ratio (=4) among hydrocarbons, the combustion of natural gas releases the least amount of carbon dioxide (CO_2) per production of unit energy (50.1 g CO_2/kJ) than the combustion of other fossil fuels (88.0–97.8 g CO_2/kJ for coal and 67.3 g CO_2/kJ for gasoline) [3]. As a result, natural gas is proposed as the only realistic solution for alleviating the carbon dioxide emissions of fossil-fuel-based power stations [4]. Other environmental benefits of natural gas combustion are the relatively low emissions of carbon monoxide, particulate matter, sulfur oxides and nitrogen oxides. Now it is widely recognized that "a Golden Age of the Gas" will begin in near future [5].

Natural gas is transported by ships or pipeline. To be transported by ships, natural gas should be liquefied under high-pressure compression, which is called liquefied natural gas (LNG). The natural gas which is transported in a gas state through pipeline is called pipeline natural gas (PNG). In general, LNG has a much higher heating value (approximately 41–42 MJ/Nm^3 [6]) than that of PNG (33.8–38.8 MJ/Nm^3) [7–9] because LNG contains more C_{2+} hydrocarbons than PNG does. South Korea and Japan import LNG by ships because they are surrounded by sea, separated from the main continent. Thus, the standard heating value of natural gas distributed in these countries is established at high values over 42.7 MJ/Nm^3. However, the average heating value of LNG in the worldwide market is on the continuous decrease because LNG suppliers tactically lower the heating value of LNG by separating C_{2+} hydrocarbons. Their purpose is first to respond to the increasing number of PNG customers by standardizing the heating values downward toward

* Corresponding author at: Department of Chemical and Biological Engineering, Korea University, Anam-dong, Seongbuk-gu, Seoul 02841, Republic of Korea.
** Co-corresponding author.
E-mail addresses: stayheavy@kangwon.ac.kr (D.-W. Lee), kylee@korea.ac.kr (K.-Y. Lee).

http://dx.doi.org/10.1016/j.molcata.2016.10.013
1381-1169/

the level of PNG and second, to make more profit by selling C_{2+} hydrocarbon gas [10]. Due to the continuous decrease in the heating value of LNG, the rate by which municipal gas distribution is measured in South Korea was recently changed from a volume-based rate to the heat-based rate. However, this practice results in an increase in the total volume consumption to meet the demanded heating values, which causes other problems, such as an increase in the cost for transport and storage.

Synthesizing high-calorie natural gas has been suggested as a solution for the problem of low-calorie natural gas. To state the obvious, the production of high-calorie gas should be based on inexpensive carbon resources, such as coal or biomass. Most existing technologies for synthetic natural gas (SNG) synthesize pure methane (*i.e.*, methanation) from coal-based synthesis gas (syngas). On the basis of the commercial SNG (methanation) processes [11], the production of high-calorie synthetic natural gas (HC-SNG) may be divided into a three-step process: (1) a coal gasifier, where coal is converted into syngas, (2) a water-gas shift (WGS) reactor to increase the H_2/CO proportion to 3, which is the stoichiometric ratio of the methanation reaction, and (3) a series of '*high-calorie SNG production*' reactors to convert the syngas into a methane and C_{2+} hydrocarbon gas mixture. The heating value of SNG can be enhanced by increasing the fraction of C_2–C_4 hydrocarbons because the heating value of individual hydrocarbons simply increases as the carbon number increases (the heating values of ethane, propane and *n*-butane are 64.3, 92.2 and 121.3 MJ/Nm^3, respectively [12]). Thus, the activity of the catalysts for the production of high-calorie SNG should be based on methanation, but at the same time, the catalyst should possess a short-chain (C_2–C_4) Fisher-Tropsch (FT) activity.

The four group VIII metals, Fe, Co, Ni and Ru, are well known to be the most active for hydrogenation of carbon monoxide to hydrocarbons [13]. Because Ni catalysts are highly selective for methane [13,14], they are not suitable for the production of high-calorie SNG. Inui et al. studied the Co-based catalyst to convert coke oven gas into high-calorie SNGs [15,16]. However, the Co-Mn-Ru/Al_2O_3 catalysts are limited in securing high C_2–C_4 selectivity. Ru has been reported to provide a strong H_2 spillover effect on the active Co phase, which resulted in increases in the CO conversion and CH_4 selectivity but also caused a decrease in the carbon chain growth [17,18]. The SNG produced using Co-Mn-Ru/Al_2O_3 contained 12.8 *vol.%* of C_2–C_4 hydrocarbons (24.6% in selectivity) to result in a heating value of 43.8 MJ/Nm^3 [18], which narrowly satisfied the required standard heating value (>42.7 MJ/Nm^3). However, this heating value is not considered high enough to mix with other low-calorie gases to increase their heating values.

Hence, we focused on Fe-based catalysts, which are known to be especially active for the production of C_2–C_4 hydrocarbons (olefins) [19–29] in FT synthesis. It was reported that a commercial Fe-based, high-temperature Fischer-Tropsch (HTFT) process produces 49 wt.% C_2–C_4 hydrocarbons with 36 wt.% gasoline and diesel [30]. Therefore, the short-chain FT activity can be regarded as an advantage of Fe when it is used as an active component of the catalyst for the production of high-calorie SNG.

The FT activity of Fe catalysts is dependent on the type of active species. Magnetite (Fe_3O_4) and various types of iron carbides (FeC_x) are known to be catalytically active in FT synthesis. Most recent studies (published in the years 2005–2015) claimed that FeC_x has higher FT activities than that of Fe_3O_4 [31–34]. However, the active phases of Fe catalysts are frequently observed to be a mixture of Fe_3O_4 and FeC_x (especially χ-Fe_5C_2). As a promoter component for Fe, Cu is a promising candidate because Cu promotes the dissociation of hydrogen (reactant) to improve the reducibility of the Fe species [35,36]. At the same time, it could act as a structural promoter to stabilize the magnetite and iron carbide phases against thermal degradation or agglomeration [37,38]. As mentioned above, Fe catalysts usually produce high olefin-to-paraffin ratio products compared to Co [39]. This is mostly due to the hydrogenation activity of Fe, which is the lowest among the first period of group VIII metals [40]. The low hydrogenation activity of Fe is *not* a disadvantage in Fischer-Tropsch applications because an otherwise high hydrogenation activity rather leads to an increase in the methane selectivity, which is unfavorable from the standpoint of FT synthesis. On the contrary, the low hydrogenation activity of the catalyst could be a disadvantage in the production of high-calorie SNG. First, it results in an increase in the olefin selectivity. It is desirable for the catalysts of the production of high-calorie SNG to maintain low olefin selectivity because an olefin has lower heating value than its analogous paraffin. Second, if a catalyst is not properly active for hydrogenation, the carbon chain growth of hydrocarbons can extend beyond an acceptable level. In SNG production, the formation of hydrocarbons longer than C_5 must be prohibited because they are condensable and cause many problems during the transportation of HC-SNG. Thus, unlike for Fischer-Tropsch catalysts, a proper level of hydrogenation activity is a type of prerequisite for the catalysts for the production of high-calorie SNG. In Fe-based catalysts, the promotion by Cu can be a way to augment the poor hydrogenation activity of Fe.

In this work, Fe-Cu catalysts were applied to the production of high-calorie SNG. The Fe-Cu catalysts were prepared by impregnating the precipitated α-Fe_2O_3 with Cu in a wide range of Fe/Cu compositions. We anticipated that CO would be activated to grow into C_2–C_4 hydrocarbons over the Fe sites, while Cu would provide the hydrogenation sites required to suppress the carbon chain growth into undesirably high hydrocarbons ($\geq C_5$) and to promote the formation of paraffin. The catalysts were activated *via* CO reduction at various temperatures, by which different types of active Fe phases were obtained, and their activities were tested in the production of high-calorie SNG. The activities were evaluated in terms of CO conversion, C_2–C_4 selectivity, chain growth probability (α), heating value (MJ/Nm^3) based on the produced hydrocarbons, *etc.* The promoting effect of Cu was examined especially in terms of the paraffin-to-olefin ratio in hydrocarbon products. Characterization techniques based on X-ray spectroscopy and temperature-programmed reduction/desorption were applied to explain the activity of the tested catalysts.

2. Materials and methods

2.1. Catalyst preparation

Fe-Cu catalysts were prepared by impregnating α-Fe_2O_3 with Cu. First, α-Fe_2O_3 was synthesized by the precipitation method as follows: 100 mL of deionized water was poured into a 500 mL three-neck flask with three necks. The water temperature was adjusted to 80 °C, and the pH was adjusted to 7 using a 1 M aqueous solution of $(NH_4)_2CO_3$ (Aldrich). Then, 60 mL of an aqueous $Fe(NO_3)_3{\cdot}9H_2O$ (Sigma-Aldrich) solution (Fe metal concentration = 1 M) was dropped into the flask at a rate of 2 mL/min. Iron hydroxides were precipitated by adding a precipitating agent, $(NH_4)_2CO_3$ (*aq.*, 1 M). The pH was maintained at 7 ± 0.03 while the precipitation continued. The precipitates were aged at 80 °C for 2 h and then washed sufficiently using 6 L of deionized water. The washed precipitates were dried at 110 °C overnight and then oxidized to α-Fe_2O_3 at 550 °C under static air for 1 h. The α-Fe_2O_3 was impregnated with Cu by the incipient wetness method using aqueous solutions of $Cu(NO_3)_2{\cdot}2.5H_2O$ (Sigma-Aldrich). The impregnated samples were dried at 110 °C overnight and calcined at 550 °C for 5 h. For convenience, Fe–Cu catalysts are abbreviated to FC catalysts, and are denoted as FC*x*-*y*R, where *x* and *y* represent the Fe/Cu ratio (*x* = 40, 15, 6) and reduction temperature (*y* = 300, 400,

Table 1
Fe/Cu atomic ratios and the Fe-Cu catalyst notation.

Catalyst	Measured atomic ratio[a](Fe/Cu)	Reduction temperature[b] (°C)	Notation
Fe_2O_3	–	not reduced	unreduced Fe_2O_3
		300	Fe_2O_3-300R
		400	Fe_2O_3-400R
		500	Fe_2O_3-500R
FC40	39.5	not reduced	unreduced **FC40**
		300	**FC40**-300R
		400	**FC40**-400R
		500	**FC40**-500R
FC15	15.0	not reduced	unreduced **FC15**
		300	**FC15**-300R
		400	**FC15**-400R
		500	**FC15**-500R
FC6	6.0	not reduced	unreduced **FC6**
		300	**FC6**-300R
		400	**FC6**-400R
		500	**FC6**-500R

[a] The concentration of each component was measured by ICP-AES.
[b] Reduced for 3 h by an 8% CO/He gas mixture at each temperature.

500 °C), respectively. The prepared catalyst notations are listed in Table 1.

2.2. Activity test

The activity of the catalysts was examined in a continuous fixed bed reactor. Each catalyst was sieved in the range of 53 to 75 μm, and 0.36 g of the catalyst was packed in the middle of a tubular stainless-steel reactor (I.D. = 9.5 mm). A catalyst was reduced at different temperatures (300, 400, 500 °C) at the ambient pressure before the reaction test with flowing 8% CO/He gas. The feed gas for the reaction tests was composed of $CO:H_2:N_2 = 24:72:4$ ($H_2/CO = 3$) and flowed into the reactor at a flow rate of 36 mL/min. The reaction pressure was maintained at 1 MPa using a back-flow regulator (TESCOM 26–1700 series, Emerson Process Management, Shanghai, China) during the entire reaction. The compositions of the feed and product gases were analyzed by gas chromatography (Younglin YL6500GC) equipped with a thermal conductivity detector (TCD) and a flame ionization detector (FID). Carboxen 1000 and HP plot Q columns were used as separation columns, which were connected to the TCD and FID, respectively. Nitrogen was used as the internal standard for determining gas compositions and the outlet flow rate. The sample gas was injected to GC without separation of water vapor but the composition of water vapor was not quantified, because it was not necessary. The CO conversion, selectivity for products, and carbon mole balance were calculated by Eqs. (1)–(4).

$$\text{CO conversion (carbon mole \%)} = \left(1 - \frac{\text{molar flow rate of unreacted CO in the product gas}}{\text{molar flow rate of CO in the feed gas}}\right) \times 100 \quad (1)$$

$$\text{Selectivity for hydrocarbons with carbon number of } n \text{ (carbon mole \%)} = \frac{n \times \text{molar flow rate of } C_n \text{ hydrocarbon in the product gas}}{\text{molar flow rate of (total carbon} - \text{unreacted CO) in the product gas}} \times 100 \quad (2)$$

$$\text{Selectivity for carbon dioxide (carbon mole \%)} = \frac{\text{molar flow rate of } CO_2 \text{ in the product gas}}{\text{molar flow rate of (total carbon} - \text{unreacted CO) in the product gas}} \times 100 \quad (3)$$

$$\text{Carbon mole balance} = \frac{\text{Total moles of carbon in the product gas per unit time}}{\text{Total moles of carbon in the feed gas per unit time}} \quad (4)$$

The chain growth probability (α) was determined from an Anderson-Schulz-Flory (ASF) plot using Eq. (5), where W_n is the mass fraction of hydrocarbons containing n carbon atoms [41].

$$\log(W_n/n) = n\log\alpha + \log[(1-\alpha)^2/\alpha] \quad (5)$$

The heating value of the SNG product gas was calculated *without* consideration of non-hydrocarbon species (H_2, CO, CO_2) in estimating the volume fractions of the hydrocarbon species (Eq. (6)) because SNG should be separated from those species in its recovery step. Among the hydrocarbon species, only the C_1–C_4 hydrocarbons were used in the heating value calculation because hydrocarbons longer than C_5 can exist in their gaseous form only if their concentration is very thin, *i.e.*, below 0.5 *vol.%* (The typical concentration of C_{5+} hydrocarbons in natural gas is below 0.34 *vol.%* [42,43].). The calculation was carried out using heat of combustion (ΔH_C) data from NIST chemistry WebBook [12].

$$\text{Heating value}\left(\text{MJ}/Nm^3\right) = \sum_{i=1}^{4}\left(x_i \times \frac{\Delta H_{C,i}}{V_{m,i}}\right) \quad (6)$$

$x_i = \text{volume fraction } C_i \text{ hydrocarbons } (i: 1-4)$

$\Delta H_{C,i} = \text{heat of combustion of } C_i \text{ hydrocarbon } \left(\text{MJ/mol}\right)$

$V_{m,i} = \text{molar volume of } C_i \text{ hydrocarbon } \left(Nm^3/\text{mol}\right)$

2.3. Characterization

Temperature-programmed reduction (TPR) analysis was carried out using a BELCAT-M-77 instrument (BEL Japan Inc.). Samples were purged at 100 °C for 1 h under a 30 mL/min flow of He gas prior to analysis. TPR data were recorded with the increase in temperature from 60 to 810 °C at 5 °C/min under a 30 mL/min flow of an 8% CO/He gas mixture (CO-TPR) at the ambient pressure. Temperature-programmed desorption (TPD) analysis was performed using the same instrument. Samples were pre-reduced at 300, 400 and 500 °C for 3 h under a 30 mL/min flow of an 8% CO/He gas mixture. For CO-TPD, CO was adsorbed on a sample at 35 °C for 30 min using an 8% CO/He gas mixture. H_2 was adsorbed *via* same procedure

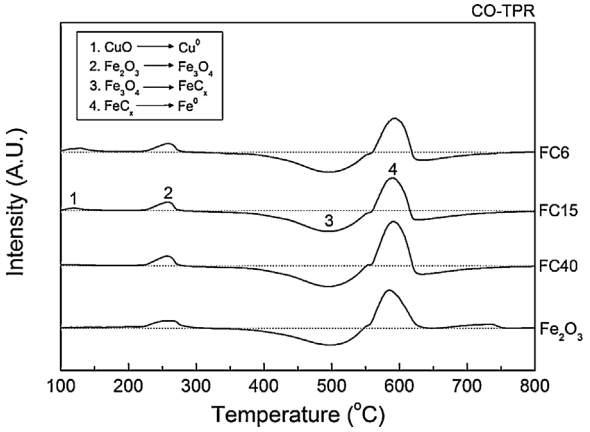

Fig. 1. CO-TPR profiles of calcined Fe-Cu catalysts (unreduced).

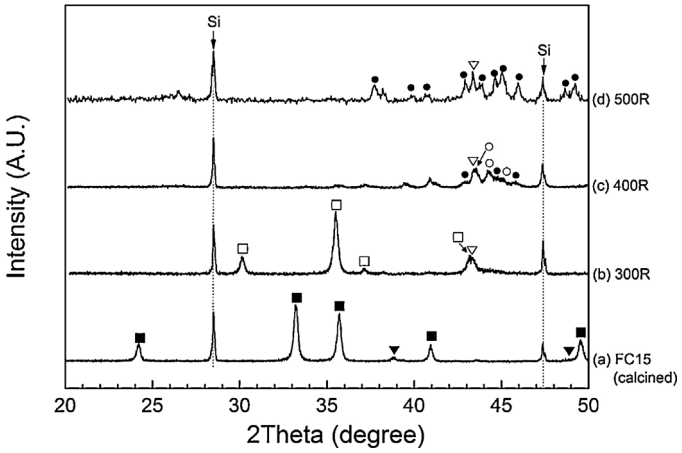

Fig. 2. X-ray diffraction results of the FC15 catalysts (a) after calcination, and CO reduction at (b) 300 °C (300R), (c) 400 °C (400R) and (d) 500 °C (500R) for 3 h: ■ α-Fe_2O_3; □ Fe_3O_4; ○ carbon-deficient FeC_x; ● Fe_3C; ▼ CuO; ▽ metallic Cu.

using a 10% H_2/He gas mixture for H_2-TPD. Physisorbed CO or H_2 molecules were removed at 120 °C for 1 h with pure He gas flowing at 30 mL/min. TPD data were recorded with the increase in temperature from 120 to 810 °C at 5 °C/min under a 30 mL/min flow of pure He gas.

X-ray diffraction (XRD) patterns were obtained using a D/MAX-2500/PC diffractometer (Rigaku) operated at 40 kV and 100 mA with Cu-Kα1 irradiation (λ = 0.15406 nm). All the samples were mixed an internal standard (Si powder) at 10 *wt.*% of total weight. The diffraction data were collected by scanning from 20 to 50° (2θ) at a rate of 1.5°/min. The domain size of the crystallites was calculated by applying the Scherrer analysis to the largest XRD peak of the crystallite (Eq. (7)) [44]. For iron carbide peaks, because their largest peaks were closely overlapping between 2θ = 43.0 and 45.1°, the Scherrer analysis was applied after peak deconvolution.

$$t = \frac{K\lambda}{B\cos\theta} \quad (7)$$

t = the mean size of the crystalline domains (nm)
K = dimensionless shape factor (= 0.9)
λ = wavelength of X-ray (Cu Kα1, 0.15406 nm)
B = full width at half maximum (FWHM) in radians
θ = Bragg angle

The mass fractions of Fe and Cu in the Fe/Cu catalysts was analyzed using an inductively coupled plasma atomic emission spectrophotometer (ICP-AES) supported by the Seoul center of the Korea Basic Science Institute (KBSI). X-ray photoelectron spectroscopy (XPS) analysis was performed on an Axis Nova instrument (Kratos) using the monochromatic Al-Kα line as X-ray source. The specific surface areas (BET areas) of the catalysts were determined *via* BET analysis using a BELSORP-max instrument (BEL Japan). Samples were degassed overnight at 4 mmHg and 100 °C prior to the analysis. N_2 adsorption was carried out at −196 °C.

3. Results and discussion

3.1. The analysis of the FC catalyst active phases

3.1.1. The change in the active Fe phases according to the reduction temperature

Fig. 1 displays the CO-TPR curves of the FC catalysts. To interpret the CO-TPR data, the oxide components of the FC catalysts should first be identified. The identification was made using XRD data (Fig. 2). Fig. 2 shows the XRD data for the FC15 catalyst, but the XRD profiles of the FC6 and FC40 catalysts (*not shown here*) were similar to those of the FC15 catalyst. The unreduced FC catalysts (FC15 (calcined), Fig. 2(a)) were composed of α-Fe_2O_3 (hematite) and CuO. On the CO-TPR run (Fig. 1), CuO was first reduced to metallic Cu near 130 °C, which was attributed to peak 1, whose intensity increased with the increasing Cu content in the catalysts. Peak 2 (~260 °C) was attributed to the reduction of α-Fe_2O_3 to Fe_3O_4 (magnetite), which was confirmed by the existence of Fe_3O_4 in the XRD results of FC15-300R (Fig. 2(b)). The carbon-deficient FeC_x species ($x < 1/3$) were detected in the XRD results when the catalyst was reduced by CO at 400 °C (FC15-400R, Fig. 2(c)), while the amount of fully carburized Fe_3C noticeably increased when the reduction temperature was raised to 500 °C (FC15-500R, Fig. 2(d)). Thus, it was deduced that Fe_3O_4 was consecutively carburized to Fe_3C *via* the carbon-deficient iron carbides (FeC_x) in the 300–500 °C section of the CO-TPR run. Therefore, peak 3 (Fig. 1), which spreads broadly over 350–550 °C, might correspond to the carburization of Fe_3O_4 to Fe_3C (*via* FeC_x). The negative signal of peak 3 is due to the differences of the CO_2/CO stoichiometry among the constituent carburization reactions, which was explained in detail in our previous publication [18]. The 2θ positions of carbon-deficient FeC_x in Fig. 2(c) (FC15-400R) were close to those of $Fe_{1.86}C_{0.14}$ (JCPDS #44-1289) and $Fe_{1.945}C_{0.055}$ (JCPDS #44-1290), but it was not strictly correct to conclude that the carbon-deficient FeC_x species were exactly composed of those two species. Thus, they were labeled collectively as "carbon-deficient FeC_x ($x < 1/3$)" in Fig. 2. Peak 4 was attributed to the reduction of Fe_3C to metallic Fe, which was supposed to take place with the precipitation of carbon [45].

In summary, the active phase of the FC catalysts changed according to the reduction temperature (300, 400 and 500 °C). The reduction sequence of Fe oxides in the CO-TPR was explained in further detail in our previous publication [18].

3.1.2. Surface properties of the reduced FC catalysts

The XPS analysis results of the reduced FC15 catalysts are presented in Fig. 3. The valance states of Fe and Cu were examined using the Fe 2p and Cu 2p XPS data. FC15-300R (Fe_3O_4) showed a single Fe $2p_{3/2}$ peak positioned at 711.0 eV. When the reduction temperature was raised (FC15-400R (FeC_x) and FC15-500R (Fe_3C)), the Fe $2p_{3/2}$ peak was divided into two, with a lower binding energy peak (707.3 eV). The lower binding energy peak was especially intense for the FC15-400R catalyst, which can be interpreted as the carbon-deficient FeC_x are more metal-like in their electron structure ($2p_{3/2}$ B.E of Fe^0 = 706.6 eV) than Fe_3O_4 and Fe_3C. Thus, an active site (Fe species, where FT carbon chain-growth might occur) of FC15-400R could be expected to be more electron-rich than those of FC15-300R and 500R. On the other hand, the Cu concentration (Cu 2p peak area) was the largest when the catalyst was reduced at the

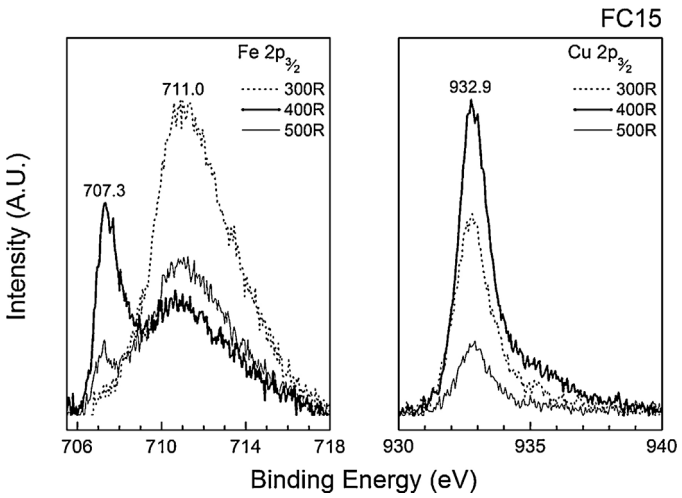

Fig. 3. Fe 2p and Cu 2p and C 1 s XPS spectra for FC15-300R, −400R, and −500R.

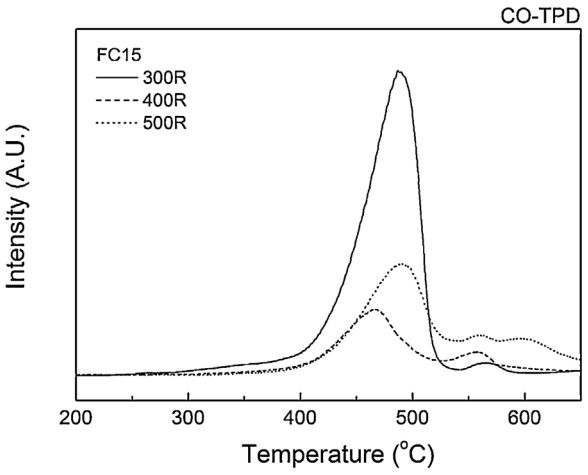

Fig. 4. CO-TPD results of FC15-300R, 400R and 500R.

middle temperature (400 °C) (FC15-300R > 400R > 500R). The effect of Cu promotion is discussed below in the chapter '*3.2. Effect of Cu on the activity of the FC catalysts*'.

A CO-TPD analysis was performed for the reduced FC catalysts, and the results are presented in Fig. 4. The total amount of adsorbed CO was the largest with FC15-300R and decreased in the order FC15-300R > 500R > 400R. However, the strong CO adsorption sites, from which CO was desorbed at a temperature higher than 550 °C, were the largest with FC15-500R, followed by FC15-400R and FC15-300R. This result implies that CO adsorption is stronger on iron carbides than on iron oxides, and the adsorption strength becomes stronger as the carburization degree of the carbide species increases. This result agrees well with the literature results: The calculations based on density functional theory (DFT) indicated that the CO adsorption energy over the (100) surface of Fe_3C ranges from −1.22 to −1.77 eV [46], while those on the Fe_3O_4 (001) surface range from −0.19 to −0.81 eV [47], which means that CO adsorbs on the Fe_3C (100) surface more easily than on Fe_3O_4 (001). Comparing carbon-deficient FeC_x (FC15-400R) with Fe_3C (FC15-400R) in the CO-TPD results, carbon-deficient FeC_x was weaker and had fewer strong chemisorption sites than Fe_3C. To summarize the CO-TPD results, the CO chemisorption strength increased in the order Fe_3O_4 < carbon-deficient FeC_x < Fe_3C.

Table 2
CO conversion, product selectivities, and carbon balance of FC catalysts after a 10 h reaction test; the reaction conditions: 300 °C, 10 bar, *w/f* = 0.01 g/mL/min, $CO:H_2:N_2$ = 24:72:4.

Catalysts	Reduction temperature (°C)	CO conv. (%)	H_2 conv. (%)	Carbon balance (%)[a]
FC40	300	85.7	36.4	99.5
	400	97.4	45.9	100.4
	500	90.5	40.5	96.0
FC15	300	94.2	43.1	99.7
	400	97.5	48.8	99.6
	500	96.6	43.6	95.5
FC6	300	84.4	34.1	99.3
	400	97.7	48.2	100.4
	500	95.4	42.4	95.9

[a] Carbon balance (%) = $\left(\frac{\text{moles of carbons ininlet flow}}{\text{moles of carbons inoutlet flow}}\right)$.

3.1.3. Catalytic activity of reduced FC catalysts in the production of high-calorie SNG

CO and H_2 conversion of FC catalysts after 10 h reaction test were listed in Table 2. Both CO and H_2 conversion were the highest in FC*x*-400R. Compared to FC*x*-300R (Fe_3O_4), FC*x*-400R (carbon-deficient iron carbides) and FC*x*-500R (Fe_3C) had stronger CO adsorption site (CO-TPD in Fig. 4), and it resulted in higher CO conversion. In addition, the BET surface of FC*x*-400R and −500R was much higher than FC*x*-300R (Table S1), it also enhanced CO conversion of iron carbide catalysts [18]. However, it seemed that CO conversion was not only influenced by the strength of CO adsorption, because FC*x*-400R achieved higher CO conversion than FC*x*-500R (Fe_3C), although FC*x*-500R had stronger CO adsorption site than FC*x*-400R (CO-TPD in Fig. 4). Because H_2 conversion was much higher in FC*x*-400R than FC*x*-500R, this higher CO conversion might be resulted from higher H_2 activation ability of FC*x*-400R (H_2-assisted conversion of CO). The surface basicity (electron donor) promotes H_2 activation [48], thus, the electron-rich state of carbon-deficient iron carbides promoted the H_2 adsorption (discussed in detail below in the chapter '*3.2. Effect of Cu on the activity of the FC catalysts*'). As a result, the electron-rich state of carbon-deficient iron carbides might cause higher H_2 activation ability of FC*x*-400R, which resulted in higher H_2 and CO conversion.

The influence of the type of Fe species on the reaction selectivity at similar CO conversion (97.2–97.5%) was examined using FC15 catalysts reduced at different temperatures, and presented in Table 3. The C_{2+} hydrocarbon selectivity (the sum of C_2–C_4 and C_{5+} selectivity) increased from 41.9% to 45.2% and 49.8% as the degree of the carburization increased (FC15-300R (Fe_3O_4-rich) < FC15-400R (carbon-deficient, FeC_x-rich) < FC15-500R (Fe_3C-rich)) while CH_4 (27.8, 26.3, and 22.1%, respectively) and CO_2 selectivity (30.3, 28.4, and 28.1%, respectively) decreased. Also, the α values showed that FC15-300R produced hydrocarbons that were relatively short in their carbon number (α = 0.15) compared to those produced by FC15-400R or 500R (α = 0.20 for both). Overall, the carbon chain growth of hydrocarbons was promoted as the carburization degree of the Fe phase increased. It is known in the literature that CO reacts with the carbon sites of iron carbides (FeC_x, Fe_3C) to form C=C=O (ketenylidene) species, which is the key intermediate of the carbon chain growth [49,50]. On the contrary, CO adsorbs as a bent or straight CO_2-like molecule on the surface of iron oxide (Fe_3O_4) [47], which is unfavorable to carbon chain growth, thus the formation of methane is promoted. Based on CO-TPD results, it was concluded that the CO chemisorption strength and the formation of C=C=O species increased as the degree of carburization increased, which resulted in the increase of the carbon chain growth in the reaction.

The carbon balance of each FC catalyst after 10 h reaction test is presented in the last column of Table 3. It shows that the balance was well preserved (99.3–100.4%) for FC*x*-300R and FC*x*-400R.

Table 3
Product distributions of FC catalysts at similar CO conversion (~97%): the reaction conditions: 300 °C, 10 bar, *w/f* = 0.01 g/mL/min, CO:H_2:N_2 = 24:72:4, reaction time for **FC15**-300R: 1 h; **FC15**-400R: 10 h; **FC15**-500R: 4 h; **FC40**-400R and **FC6**-400R: 10 h.

	Reduction temp. (°C)	CO conv. (%)	Selectivity (%)								α[b]	p/o[c]
			CH_4	C_2–C_4					C_{5+}	CO_2		
				C_2H_6	C_2H_4	C_3H_8	C_3H_6	C_4H_{10}[a]	C_4H_8			
FC15	300	97.2	27.8	34.4						7.5	30.3	0.15	2.04
				10.6	1.5	6.8	7.1	4.1	4.3				
	400	**97.5**	26.4	34.4						10.8	28.4	0.20	2.51
				9.9	0.9	8.1	6.5	5.3	3.7				
	500	**97.5**	22.1	36.6						13.2	28.1	0.20	1.63
				9.4	1.5	6.6	9.0	5.1	5.0				
FC40	400	**97.4**	25.8	34.6						9.6	30.0	0.19	1.98
				9.6	1.4	7.2	7.4	4.7	4.3				
FC15		**97.5**	26.4	34.4						10.8	28.4	0.20	2.51
				9.9	0.9	8.1	6.5	5.3	3.7				
FC6		**97.7**	25.3	34.6						11.2	28.9	0.19	2.04
				9.8	1.3	7.3	7.3	4.7	4.2				

[a] Only *n*-C_4H_{10} was detected.
[b] The α values of the FC catalysts were calculated based on the Anderson-Flory-Shultz distribution in the C_1–C_6 range.
[c] The molar ratio of paraffin to olefin in C_2–C_4 fractions.

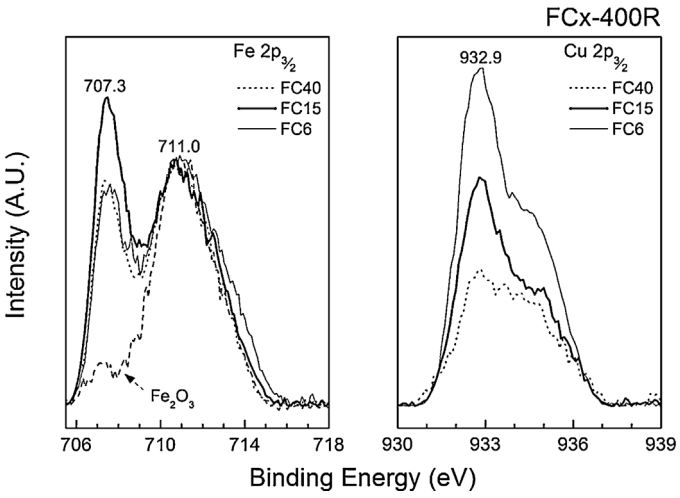

Fig. 5. Fe 2p and Cu 2p and C 1 s XPS spectra for FC40, FC15 and FC6-400R.

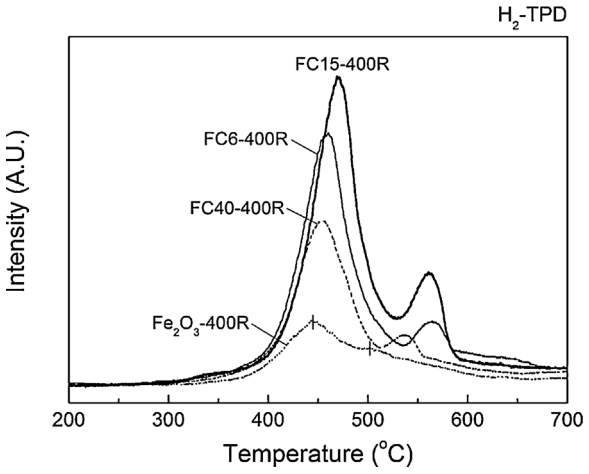

Fig. 6. H_2-TPD results of FC*x*-400R (*x* = 40, 15, 6) and pure Fe_2O_3.

FC*x*-500R was slightly deficient in the carbon balance (95.5–96.0%), which might be due to the occurrence of coke formation on the catalyst surface. It implies that the strong chemisorption of CO might cause a coking problem. A Fischer-Tropsch study revealed that the rate of coke deposition increases as the carburization degree of the Fe phase increases (θ-Fe_3C < χ-Fe_5C_2 < ε-$Fe_{2.2}C$) [51]. This agrees well with the carbon balance of the reaction results in our study (Table 3): FC*x*-300R and −400R were almost 100% in carbon balance, whereas FC*x*-500R (Fe_3C), which had the highest carburization degree, was deficient by 4% from having a perfect carbon balance.

In summary, the CO conversion was the highest with FC15-400R, while the highest hydrocarbon selectivity and yield were achieved using FC15-500R. During the 10 h reaction tests, the coke deposition was almost absent except FC*x*-500R catalysts.

3.2. Effect of Cu on the activity of the FC catalysts

3.2.1. The influence of Cu loading on surface properties of the reduced FC catalysts

Fig. 5 presents the XPS analysis results of the FC*x*-400R (*x* = 40, 15 and 6) catalysts. First, the peak for a metal-like Fe (707.3 eV) in Fe_2O_3-400R (without Cu) was much smaller than those in FC*x*-400R, which indicated that the metal-like, electron-rich Fe site were generated by the Cu promotion. The ratio between the peak for a metal-like Fe and that for normal Fe (711.0 eV) was differed by the Fe/Cu ratio, and was the largest in FC15-400R, while the Cu concentration on the surface simply increased as Cu/Fe ratio increased (Fe/Cu ratio decreased). Because the carbon concentration on the surface of FC*x*-400R catalysts was the largest in FC15-400R (Table S2), it implies that the electron-rich Fe*Cx* was generated by hindering the carbon incorporation and Fe-C bond formation during the pre-reduction. It also implies that Cu blocked the carbon incorporation, but it is not clear why the electron-rich Fe*Cx* was the most abundant in FC15-400R. This order might be associated with how the thermal agglomeration of copper (Tamman temperature of Cu ≈ 500 °C) is balanced by its interaction with the iron species on the catalyst surface.

Fig. 6 presents the H_2-TPD results of the FC catalysts reduced at 400 °C. Two peaks appeared in all samples at 450–500 °C and at over 500 °C. It was observed that Fe_2O_3-400R also chemisorbed H_2, but the chemisorption increased (*i.e.*, the peak intensity increased) and became stronger (*i.e.*, the peak temperature increased) as the Cu loading of the catalyst increased. As mentioned above, the electron-rich surface promoted the adsorption of H_2 [48], thus, the amount of chemisorbed H_2 was the largest in FC15-400R, which had the most electron-rich Fe site. For FC40-400R and FC6-400R, XPS spectra of Fe for these two catalysts were almost identical, but the amount of chemisorbed H_2 was larger on FC6-400R than FC40-400R. Because

Table 4
Calculated heating values of the product gases.

Catalyst	Heating value of the product gas[a]	Product gas composition (vol%; without N_2[b], H_2O[c])	
FC15-300R	52.3 MJ/Nm^3	**H_2**	**69.7**
		CO_x	14.8
		Hydrocarbons	15.5
FC15-400R	53.4 MJ/Nm^3	**H_2**	**68.7**
		CO_x	13.5
		Hydrocarbons	17.8
FC15-500R	56.4 MJ/Nm^3	**H_2**	**71.4**
		CO_x	13.5
		Hydrocarbons	15.1

[a] The heating values were calculated considering C_1–C_4 fractions only. The values are meaningful because C_{5+} fractions are minor in amount, and all the non-hydrocarbon species will be separated in the recovery of SNG.
[b] N_2 was included as an internal standard for GC analysis.
[c] $H_2O(v)$ was assumed to be separated.

Table 5
H_2 conversion and moles of H_2 converted and generated during the reaction using FC15 catalysts; the reaction conditions: 300 °C; 1 MPa; *w/f* = 0.01 g/mL/min; feed composition $CO:H_2:N_2$ = 24:72:4.

	Reduction temperature (°C)	Time on Stream	CO conv. (%)	H_2 conv. (%)	*p/o*[a]	α[b]	The amount of H_2 in the flow stream (mmol/min)			
							H_2 input (feed)	Converted by hydrogenation of CO	Generated by WGSR	Remaining in the product stream
FC15	300	1 h	97.2	51.8	2.04	0.15	1.059	0.662	0.114	0.511
	400	10 h	97.5	48.8	2.51	0.20		0.614	0.097	0.542
	500	4 h	97.5	46.9	1.63	0.20		0.593	0.096	0.562

[a] The molar ratio of paraffin to olefin in C_2–C_4 fractions.
[b] The α values of the FC catalysts were calculated based on the Anderson-Flory-Shultz distribution in the C_1–C_6 range.

the surface Cu concentration was larger in FC6-400R than FC40-400R, it implies that H_2 also chemisorbed on Cu sites.

3.2.2. *The influence of Cu loading on the activity of the reduced FC catalysts*

The influence of Cu loading on the product selectivity was examined using FC*x*-400R catalysts. The CO conversion was adjusted at ca. 97% by allowing a different reaction time for each catalyst. The results are presented in Table 3, showing the product selectivity did not change much according to the Cu loading of the catalysts. However, the *p/o* ratio increased in the order FC15 > FC6 > FC40 (from the tests of FC*x*-400R, Table 3), which was identical to the order of the catalysts regarding the H_2 adsorption amount (peak areas) in the H_2-TPD tests (Fig. 6). These results imply that the major role of adsorbed H_2 was to saturate olefins rather than to restrict the carbon chain growth of hydrocarbons.

In summary, the *p/o* ratio was the highest with FC15-400R, which was the most prominent for its H_2 adsorption. Therefore, the impregnation of Cu was deduced to not be as effective as the change in the Fe active phase at improving C_2–C_4 selectivity, but it was effective at increasing the paraffin-to-olefin (*p/o*) ratio of hydrocarbon products.

3.3. *Evaluation of heating values for the produced SNG gases*

Table 4 presents the heating values of the product gases of the FC15 catalysts reduced at different temperatures. Excluding the contributions from non-hydrocarbon gases (H_2, CO_x, and H_2O), and C_{5+} hydrocarbons, the heating values of the product gases (SNG fraction, C_1–C_4) were in the range of 52.3–56.4 MJ/Nm^3, which exceeds the standard heating value (41–44.4 MJ/Nm^3) of the natural gas currently distributed over South Korea. However, the product gases contained very high concentrations of remaining H_2 (68.7–71.4 *vol.%* for FC15 catalysts, N_2-free and dry basis). This is unavoidable in HC-SNG synthesis because the unreacted hydrogen always remains if C_n ($n > 2$) hydrocarbons are formed from feed gas with a H_2/CO ratio of 3. Basically, the concentration of remaining H_2 is inversely proportional to CO conversion (*i.e.*, H_2 conversion increases as the CO conversion increases): the H_2 conversion was in the same order of CO conversion (Table 2). At similar CO conversions (shown in Table 5), the concentration of remaining H_2 is determined according to the carbon chain growth (α) and the paraffin-to-olefin ratio (*p/o*) of the hydrocarbon fraction of a product gas. First, the increase in the carbon chain growth (α) lowered the H_2 conversion. As given in Eqs. (8) and (9), the molar ratio of H_2/CO (converted) is between 2 ($n = \infty$) and 3 ($n = 1$).

$$nCO + (2n+1)H_2 \rightarrow C_nH_{2n+2} + nH_2O \quad (8)$$

(H_2/CO (converted) = $2 + 1/n$ for production of paraffins)

$$nCO + 2nH_2 \rightarrow C_nH_{2n} + nH_2O \quad (H_2/CO(\text{converted}) = 2 \text{ for production of olefins}) \quad (9)$$

Because the molar ratio of H_2/CO (converted) decreases as the carbon number of produced paraffin (n) increases (Eq. (8)), the concentration of the remaining hydrogen increases as the carbon chain growth (α) increases only if the CO conversion is fixed at a certain value. This fixed value corresponds to the data in Table 5, in which the amount of H_2 converted by hydrogenation of CO decreased from 0.662 to 0.614 mmol/min as the α value increased from 0.15 (FC15-300R in 1 h reaction) to 0.20 (FC15-400R in 10 h reaction). In the cases of producing olefins, the molar ratio of H_2/CO (converted) is always 2, regardless of the carbon number of the olefin (Eq. (9)). Thus, an increase in the olefin selectivity would accompany a slight decline in the H_2 conversion. This trend corresponds well to the aforementioned data of Table 5: the amount of H_2 converted by the hydrogenation of CO decreased from 0.614 to 0.593 mmol/min as the *p/o* ratio decreased from 2.51 (FC15-400R with a 1 h reaction) to 1.63 (FC15-500R with a 4 h reaction).

The concentration of the remaining hydrogen is also influenced by the degree to which the water-gas shift reaction (WGSR) progressed over the catalyst. Fe-Cu catalysts are well known for their WGSR activity [52–56]. Hence, H_2 can be generated *in situ* by the

parallel occurrence of the WGSR (Eq. (10)) during the production of high-calorie SNG. The generated moles of H_2 by WGSR could be calculated directly from the moles of CO_2 in the product gas. CO_2 can also be generated *via* the Boudouard reaction (CO disproportionation) (Eq. (11)), producing solid carbon as a co-product. However, the formation of solid coke was considered negligible because the carbon balances were close to 100% for most of the catalysts (Table 2). Therefore, the contribution of the Boudouard reaction was disregarded in the analysis of the WGSR that occurred over the FC_x catalysts.

$$CO + H_2O \rightarrow CO_2 + H_2 \quad (10)$$

$$2CO \rightarrow C + CO_2 \quad (11)$$

Finally, the amount of remaining H_2 in the product gas could be attained by subtracting the amount of converted H_2 from the CO hydrogenation from the amount of H_2 in the feed and adding the amount of generated H_2 *via* WGSR. Table 5 shows that most of the remaining H_2 (mmol/min) was from the unreacted H_2, and the contribution of WGSR-generated H_2 was comparatively small. Therefore, it could be summarized that the carbon chain growth and the olefin formation can mostly be attributed to the high concentration of remaining H_2 in the high-calorie product gas.

The fact that a high concentration of remaining H_2 is unavoidable means a post-process such as hydrogen recovery or additional methanation should be considered in designing or installing HC-SNG production facilities. The use of post-methanation reactor units is the most promising method because it not only reduces H_2 concentration but also makes additional methane. In general, the commercial methanation processes consist of 2–6 methanation reactors, which can obtain nearly complete conversions of hydrogen and carbon oxides [11]. The methanation reactors are linked *via* an optimized set of recycle or bypass streams. For example, recycling a part of product stream into the feed stream is recommended for the first methanation reactor because the first methanation reactor requires a feed with a high H_2/CO ratio (=3), and its product stream is more H_2-rich than those of following methanation reactors. The product stream of high-calorie SNG is much more H_2-rich ($H_2/CO = 29.4–61.4$) than those of simple methanation. If such a H_2-rich product stream is recycled to the first reactor, it would be possible to reduce the size of the WGSR unit (or to remove the unit, in the best-case scenario), which is positioned in front of the first methanation unit to adjust the H_2/CO ratio for methanation. In addition, a part of the feed gas (a synthesis gas from a coal gasification unit, which is relatively CO-rich, $H_2/CO = \sim 1$) to the WGSR reactor can be by-passed to the feed stream to the post-methanation reactors, by which the H_2/CO ratio required for the reactors can be adjusted (3, most desirably).

4. Conclusions

In this work, the activity of Fe-Cu catalysts in the production of high-calorie SNG was investigated. The major active Fe phase of the Fe-Cu catalysts changed according to the CO reduction (pre-treatment) temperature: Fe_3O_4 at 300 °C, carbon-deficient FeC_x at 400 °C and Fe_3C at 500 °C. The carburization of iron oxide resulted in stronger CO adsorption and higher BET surface area, as a result, iron carbide catalysts (FC*x*-400R and −500R) achieved higher conversion than Fe_3O_4 (FC-300R). Also, the carbon-deficient FeC_x was metal-like in its electron structure due to the low number of bonded carbons, and it was attributed to the highest CO and H_2 conversion of FC15-400R by providing H_2 activation ability. For product selectivity, the production of C_n ($n > 2$) hydrocarbons increased as the degree of carburization increased: FC15-500R > 400R > 300R. As the degree of carburization increased (Fe_3C > carbon-deficient FeC_x > Fe_3O_4), the chemisorption strength of CO also increased, which consequently resulted in an increase in the carbon chain growth of hydrocarbons. On the other hand, the loading amount of Cu exerted little influence on the product selectivity, but the impregnated Cu promoted H_2 adsorption, leading to an increase in the *p/o* ratio of the produced hydrocarbons. As a result, the heating values of the SNGs produced by Fe-Cu catalysts were estimated to be 52.3–56.4 MJ/Nm^3, which satisfied the heating value standard of commercial LNG distributed over South Korea.

Acknowledgments

This work was supported by the National Research Foundation of Korea (NRF) grant funded by the Korea government (MSIP) (NRF-2015R1A2A1A13001856).

Appendix A. Supplementary data

Supplementary data associated with this article can be found, in the online version, at http://dx.doi.org/10.1016/j.molcata.2016.10.013.

References

[1] World Energy Outlook 2015, International Energy Agency, 2015.
[2] Statistical Review of World Energy, British Petroleum Company, 2015.
[3] How much carbon dioxide is produced when different fuels are burned?, U.S. Energy Information Administration (EIA), 2016.
[4] R. Muller, Energy for Future Presidents: The Science Behind the Headlines, 1st ed., W.W. Norton, New York, 2012.
[5] World Energy Outlook 2011, International Energy Agency, 2011.
[6] Y. Nishiyama, Energy in Japan: On the Introduction of Shale Gas, Credit Suisse, 2012.
[7] Heat Content of Natural Gas Consumed, U.S. Energy Information Administration (EIA), 2015.
[8] M. Korchemkin, Gazprom Unlikely to Win a Price War, East European Gas Analysis (EEGA), 2016.
[9] Gazprom, Scale Does Matter: Gazprom Investor Day, 2012.
[10] Description of the city gas calories system documentation, Korea Gas Corporation (KOGAS), 2012.
[11] J. Kopyscinski, T.J. Schildhauer, S.M.A. Biollaz, Fuel 89 (2010) 1763–1783.
[12] National Institute of Standards and Technology (U.S.), NIST chemistry webbook, in: NIST Standard Reference Database 69, National Institute of Standards and Technology, Washington, D.C, 2016.
[13] M.E. Dry, FT catalysts, in: M.E. Dry, A.P. Steynberg (Eds.), Fischer-Tropsch Technology, 2004, pp. 533–600.
[14] B.C. Enger, A. Holmen, Catal. Rev. 54 (2012) 437–488.
[15] T. Inui, A. Sakamoto, T. Takeguchi, Y. Ishigaki, Ind. Eng. Chem. Res. 28 (1989) 427–431.
[16] Y. Ishigaki, M. Uba, S. Nishida, T. Inui, Appl. Catal. 47 (1989) 197–208.
[17] Y.H. Lee, H. Kim, H.S. Choi, D.W. Lee, K.Y. Lee, Korean J. Chem. Eng. 32 (2015) 2220–2226.
[18] Y.H. Lee, D.-W. Lee, H. Kim, H.S. Choi, K.-Y. Lee, Fuel 159 (2015) 259–268.
[19] H.M.T. Galvis, J.H. Bitter, C.B. Khare, M. Ruitenbeek, A.I. Dugulan, K.P. de Jong, Science 335 (2012) 835–838.
[20] J.Z. Lu, L.J. Yang, B.L. Xu, Q. Wu, D. Zhang, S.J. Yuan, Y. Zhai, X.Z. Wang, Y.N. Fan, Z. Hu, ACS Catal. 4 (2014) 613–621.
[21] N. Jiang, G.H. Yang, X.F. Zhang, L. Wang, C.Y. Shi, N. Tsubaki, Catal. Commun. 12 (2011) 951–954.
[22] X.Q. Chen, D.H. Deng, X.L. Pan, Y.F. Hu, X.H. Bao, Chem. Commun. 51 (2015) 217–220.
[23] Y. Liu, J.F. Chen, J. Bao, Y. Zhang, ACS Catal. 5 (2015) 3905–3909.
[24] H.M.T. Galvis, J.H. Bitter, T. Davidian, M. Ruitenbeek, A.I. Dugulan, K.P. de Jong, J. Am. Chem. Soc. 134 (2012) 16207–16215.
[25] S.H. Kang, J.W. Bae, P.S.S. Prasad, K.W. Jun, Catal. Lett. 125 (2008) 264–270.
[26] Z.Q. Yang, X.L. Pan, J.H. Wang, X.H. Bao, Catal. Today 186 (2012) 121–127.
[27] Y. Liu, J.F. Chen, Y. Zhang, RSC Adv. 5 (2015) 29002–29007.
[28] C. Wang, Q.X. Wang, X.D. Sun, L.Y. Xu, Catal. Lett. 105 (2005) 93–101.
[29] J.D. Xu, K.T. Zhu, X.F. Weng, W.Z. Weng, C.J. Huang, H.L. Wan, Catal. Today 215 (2013) 86–94.
[30] M.E. Dry, A.P. Steynberg, Commercial FT process applications, in: M.E. Dry, A.P. Steynberg (Eds.), Fischer-Tropsch Technology, 2004, pp. 406–481.
[31] A. Sarkar, D. Seth, A.K. Dozier, J.K. Neathery, H.H. Hamdeh, B.H. Davis, Catal. Lett. 117 (2007) 1–17.
[32] M.Y. Ding, Y. Yang, B.S. Wu, J. Xu, C.H. Zhang, H.W. Xiang, Y.W. Li, J. Mol. Catal. A-Chem. 303 (2009) 65–71.
[33] M.S. Luo, H. Hamdeh, B.H. Davis, Catal. Today 140 (2009) 127–134.
[34] M.Y. Ding, Y. Yang, Y.W. Li, T.J. Wang, L.L. Ma, C.Z. Wu, Appl. Energy 112 (2013) 1241–1246.

[35] C.-H. Zhang, Y. Yang, B.-T. Teng, T.-Z. Li, H.-Y. Zheng, H.-W. Xiang, Y.-W. Li, J. Catal. 237 (2006) 405–415.
[36] K.-D. Jung, A.T. Bell, J. Catal. 193 (2000) 207–223.
[37] S. Li, W. Ding, G.D. Meitzner, E. Iglesia, J. Phys. Chem. B 106 (2002) 85–91.
[38] S. Li, S. Krishnamoorthy, A. Li, G.D. Meitzner, E. Iglesia, J. Catal. 206 (2002) 202–217.
[39] H. Schultz, Fischer-Tropsch synthesis in a modern perspective, in: A. Beller (Ed.), Catalysis: From Principles to Applications, 2011.
[40] C.N. Satterfield, Heterogeneous Catalysis in Industrial Practice, 2nd ed., McGraw-Hill, New York, 1991.
[41] Y. Liu, J. Luo, J. Girleanu, O. Ersen, C. Pham-Huu, C. Meny, J. Catal. 318 (2014) 179–192.
[42] A. Demirbas, Methane Gas Hydrate, Springer, London; New York, 2010.
[43] Sasol, Natural Gas: Addendum to specification.
[44] B.D. Cullity, Elements of X-ray Diffraction, Addison-Wesley Pub Co., Reading, Mass, 1956.
[45] G. Routschka, Refractory Materials: Pocket Manual; Design, Properties, Testing, 3rd ed., Vulkan-Verlag GmbH, 2008, 2016.
[46] J.G. Wang, H.J. Jian, J. Mol. Catal. A-Chem. 269 (2007) 169–178.
[47] P.Y. Xue, Z.M. Fu, X.L. Chu, Y.X. Zhang, Z.X. Yang, Appl. Surf. Sci. 317 (2014) 752–759.
[48] A. Travert, H. Nakamura, R.A. van Santen, S. Cristol, J.F. Paul, E. Payen, J. Am. Chem. Soc. 124 (2002) 7084–7095.
[49] J.W. Kolis, E.M. Holt, D.F. Shriver, J. Am. Chem. Soc. 105 (1983) 7307–7313.
[50] W.C. Wu, Z.L. Wu, C.H. Liang, X.W. Chen, P.L. Ying, C. Li, J. Phys. Chem. B 107 (2003) 7088–7094.
[51] A. Machocki, Appl. Catal. 70 (1991) 237–252.
[52] A. Khan, P.G. Smirniotis, J. Mol. Catal. A-Chem. 280 (2008) 43–51.
[53] M. Estrella, L. Barrio, G. Zhou, X.Q. Wang, Q. Wang, W. Wen, J.C. Hanson, A.I. Frenkel, J.A. Rodriguez, J. Phys. Chem. C 113 (2009) 14411–14417.
[54] L.Z. Zhang, J.M.M. Millet, U.S. Ozkan, Appl. Catal. A-Gen. 357 (2009) 66–72.
[55] D.W. Jeong, V. Subramanian, J.O. Shim, W.J. Jang, Y.C. Seo, H.S. Roh, J.H. Gu, Y.T. Lim, Catal. Lett. 143 (2013) 438–444.
[56] Z.H. Bao, W.Z. Ding, Q. Li, Int. J. Hydrogen Energy 37 (2012) 951–955.